Epithelial Responses in Radiation-Induced Lung Injury (RILI) Allow Chronic Inflammation and Fibrogenesis

Authors: Beach, Tyler A., Finkelstein, Jacob N., and Chang, Polly Y.

Epithelial Responses in Radiation-Induced Lung Injury (RILI) Allow Chronic Inflammation and Fibrogenesis

Tyler A. Beach,[a] Jacob N. Finkelstein,[b] Polly Y. Chang[a,1]

[a]SRI Biosciences, SRI International, Menlo Park, Calfornia 94025-3493; [b]University of Rochester Medical Center, Departments of Pediatrics and Neonatology, and Environmental Medicine, Rochester, New York 14642

Beach TA, Finkelstein JN, Chang PY. Epithelial Responses in Radiation-Induced Lung Injury Allow Chronic Inflammation and Fibrogenesis. Radiat Res. 199, 439–451 (2023).

Radiation models, such as whole thorax lung irradiation (WTLI) or partial-body irradiation (PBI) with bone-marrow sparing, have shown that affected lung tissue displays a continual progression of injury, often for months after the initial insult. Undoubtedly, a variety of resident and infiltrating cell types either contribute to or fail to resolve this type of progressive injury, which in lung tissue, often develops into lethal and irreversible radiation-induced pulmonary fibrosis (RIPF), indicating a failure of the lung to return to a homeostatic state. Resident pulmonary epithelium, which are present at the time of irradiation and persist long after the initial insult, play a key role in the maintenance of homeostatic conditions in the lung and have often been described as contributing to the progression of radiation-induced lung injury (RILI). In this study, we took an unbiased approach through RNA sequencing to determine the in vivo response of the lung epithelium in the progression of RIPF. In our methodology, we isolated CD326+ epithelium from the lungs of 12.5 Gy WTLI C57BL/6J female mice (aged 8–10 weeks and sacrificed at regular intervals) and compared irradiated and non-irradiated CD326+ cells and whole lung tissue. We subsequently verified our findings by qPCR and immunohistochemistry. Transcripts associated with epithelial regulation of immune responses and fibroblast activation were significantly reduced in irradiated animals at 4 weeks postirradiation. Additionally, alveolar type-2 epithelial cells (AEC2) appeared to be significantly reduced in number at 4 weeks and thereafter based on the diminished expression of pro-surfactant protein C (pro-SPC). This change is associated with a reduction of Cd200 and cyclooxygenase 2 (COX2), which are expressed within the CD326 populations of cells and function to suppress macrophage and fibroblast activation under steady-state conditions, respectively. These data indicate that either preventing epithelial cell loss that occurs after irradiation or replacing important mediators of immune and fibroblast activity produced by the epithelium are potentially important strategies for preventing or treating this unique injury.   © 2023 by Radiation Research Society

[1] Corresponding author address: SRI Biosciences, SRI International, 333 Ravenswood Ave., Menlo Park, CA 94025-3493; email: polly.chang@sri.com.

INTRODUCTION

Pulmonary fibrosis (PF) is characterized by the accumulation of extracellular matrix (ECM), which disrupts normal tissue structure and can progressively lead to loss of lung function. A number of stimuli can initiate PF, such as exogenous exposure to asbestos, sulphur mustard gas, bleomycin, amiodarone, and medical or accidental radiation exposure, and endogenous factors including autoimmune disease and sporadic or familial gene mutations. Chronic or persistent epithelial injury is thought to underlie many forms of pulmonary fibrosis (1–4) including RIPF (5, 6). Experimental models support this notion as chronic depletion of club cells lining the small airways (7) or persistent injury to AEC2 (1) are sufficient to induce the formation of fibrotic foci. Examining lung tissue obtained in a well described model of RIPF that reliably results in radiation pneumonitis and fibrosis (8–12) established that chronic oxidative stress, cellular senescence, and the presence of DNA damage in lung tissue can be detected months after the initial exposure to ionizing radiation (9). These factors indicate a pulmonary environment conducive to further cellular injury and genomic damage, which may alter the normal function of resident epithelial cells after irradiation.

Pulmonary epithelial cells, particularly club cells and AEC2s, play a critical role in the maintenance of tissue homeostasis. Both cells function as a type of adult stem cells able to self-renew to maintain populations long-term, give rise to different cell types during normal turnover, and replace damaged cells after injury (13). Club cells can differentiate into ciliated epithelia located in the bronchiole and bronchoalveolar stem cells (BASCs) located at the bronchoalveolar junction, and BASCs can give rise to AEC2s, which reside within the alveoli (13). In similar fashion, surfactant producing, pro-SPC-positive, AEC2 cells can transdifferentiate into squamous AEC type-1 cells lining the alveoli in response to injury (14); thus, both club cells and AEC cell types contribute to maintaining the epithelial barrier of bronchioles and alveoli. Also, these epithelia secrete Club cell secretory protein (CCSP) and surfactant proteins (-A,-B,-C,-D), which further support

439

alveolar structure preventing atelectasis, allow for effective gas exchange, and bolster innate immunity through the activity of collectins (surfactants -A and -D) that agglutinate a variety of bacteria, viruses, and fungi for effective opsonization by phagocytic cells (15). CCSP has also been shown to inhibit monocyte, neutrophil, and fibroblast chemotaxis (16), and it may play a role in the attenuation of inflammatory and fibrotic responses. In addition to surfactants and secretoglobins, the epithelium is thought to produce factors important to regulating the actions of other cell types present, especially immune cells and fibroblasts, which play an important part in the development of RIPF. Examples relevant to epithelial cells include CD200 (17) and PGE$_2$ (18).

CD200, which is endogenously expressed by pulmonary epithelia, is a ligand that interacts with the CD200 receptor (CD200r), which is highly expressed on alveolar macrophages. Through this interaction, pulmonary epithelia inhibit myeloid cell activation (19), which may act to reduce myeloid cell production of inflammatory factors such as TNFα, IL-6, and possibly macrophage-mediated ROS production. Co-culture experiments have shown that the expression of CD200 by airway epithelia suppresses TNFα and IL-6 production of γ-Interferon-stimulated macrophages. Furthermore, CD200$^{-/-}$ mice display an exaggerated inflammatory response when exposed to influenza (17). These examples demonstrate the importance of the CD200/200r interaction in the resolution of inflammation.

In addition to interacting with myeloid cells, AEC2s have been shown to influence fibroblast activity under steady-state conditions via the synthesis of prostaglandin E$_2$ (PGE$_2$) via the activity of cyclooxygenase (COX) enzymes. There are two isoforms of the COX enzyme, COX1 and COX2, and while both are constitutively active in lung epithelia, COX2 is primarily responsible for the synthesis of PGE$_2$ and the antifibrotic actions of AEC2s (20). PGE$_2$ is an endogenous inhibitor of fibroblast functions including chemotaxis (21), proliferation (22, 23), collagen production (24), and differentiation into myofibroblasts (23). In this way, PGE$_2$ plays an important role in mediating homeostasis in the lungs (18) and preventing the development of a profibrotic fibroblast phenotype (23). Clinically, pulmonary fibrosis patients have been found to have significantly reduced levels of PGE$_2$ in epithelial lining fluid (25).

Due to the importance of AEC2 cells in the maintenance of homeostatic conditions and regulation of other cell types present in the lung, we sought to quantify changes in the numbers of pro-SPC expressing AEC2 cells throughout the progression of RILI and to determine how or if the expression of important regulatory genes and/or proteins associated with this population can be changed within the epithelium after irradiation. To examine the epithelial response after 12.5 Gy WTLI, we collected whole lung tissue and pulmonary epithelial cells of irradiated and non-irradiated C57BL6/J mice sacrificed at scheduled intervals

up to 32 weeks postirradiation and interrogated these tissues through low-input RNA sequencing, qPCR, and histochemistry. We also compared the histology of this 12.5 Gy WTLI model, which was previously shown to develop RIPF (8–11), to a prior experiment using 10 Gy WTLI in which the mice did not appear to develop lethal RIPF (26).

To interrogate the transcriptional response of lung epithelial cells, we developed a method to rapidly isolate CD326 (EpCam) positive epithelial cells from whole lung-tissue digest for RNA isolation, and compared irradiated whole lung tissue or epithelial cells to non-irradiated tissue or cells (Fig. 1). This technique reveals transcriptional changes occurring in vivo, and based on tissues collected at multiple time points, represents changes occurring during the onset and progression of RILI. Furthermore, by comparing transcripts obtained from epithelial cells to those present in whole tissue in the non-irradiated condition, we were able to identify a number of genes responsible for the expression of important proteins that were likely to be produced specifically in epithelial cells of the lung and determine how the expression of these transcripts were altered in response to radiation over time. RNA-sequencing comparisons provided an unbiased approach to the interrogation of transcriptional changes occurring in the progression of injury in whole lung tissue and within the epithelial population, which could be subsequently verified through qPCR and histology. The goal for the experiments presented in this manuscript was to identify an epithelial phenotype that triggers and maintains persistent tissue dysfunction to identify potential methods to prevent or treat late effects of pulmonary radiation injury.

METHODS

Animals

We obtained female C57BL/6J mice, 6–8 weeks of age from Jackson Laboratory (Bar Harbor, ME) and acclimated 5 animals per cage under controlled conditions up to 2 weeks prior to experimentation. We euthanized animals (intraperitoneal injection of sodium pentobarbital) at 24 h and at 1, 4, 12, 16, 24, and 32 weeks postirradiation and used their excised lungs for immunohistochemistry and RNA isolation. Twelve animals were assigned to each treatment group for each examination time point, and all animals received a standard laboratory diet and water ad libitum. All experiments were performed under protocols approved by the University of Rochester Committee on Animal Resources.

Irradiation

Unanesthetized animals were restrained in plastic jigs placed so that the thoraxes were in the field defined by a lead collimator and irradiated with 12.5 Gy or 10 Gy (thorax only) using a ^{137}Cs γ-ray source operating at a dose rate of approximately 1.5 Gy/min. Age-matched non-irradiated (0 Gy) control mice received similar handling.

Lung Histology and Immunohistochemistry Analysis

For histological examination, lungs were inflated, excised, fixed in 10% buffered zinc formalin (Anatech, Battle Creek, MI) and paraffin embedded. At 0 and 12.5 Gy, 3 animals were collected for each time
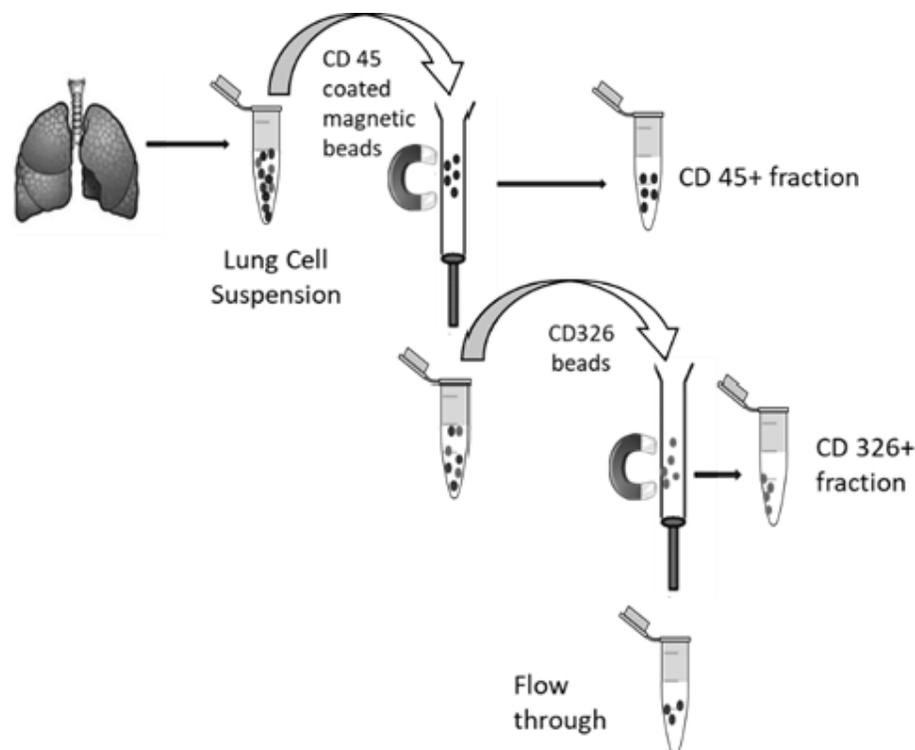
FIG. 1. Epithelial cell isolation for qPCR and low input RNA seq. Using antibody-coated magnetic microbeads, CD45-positive cells were depleted from whole lung tissue digest. Cells not captured by CD45 beads were then incubated with CD326-coated beads, which allowed for the capture of CD326-positive cells from the CD45-depleted lung tissue digest.

point and treatment group (n = 3). Only 2 animals were available per time point in the 10 Gy group (n = 2) and had been sacrificed as part of an earlier experiment. Non-irradiated (0 Gy) animals were examined at 1, 12 or 16, and 32 weeks for comparisons to irradiated groups of similar age during the acute, mid, and late timepoints, as there was little discernable change and no pathology observed in the lungs of sham animals over the course of the experiment.

Quantitation of type 2 AECs was performed using brightfield microscopy to determine the number of AECs per alveolus, and fluorescence microscopy was used for dual staining with cyclooxygenase 2 (COX 2).

For brightfield imaging, deparaffinized tissue sections (6 μm) were treated to block endogenous peroxidases followed by antigen retrieval in citrate buffer (Dako, Glostrup, Denmark) and blocking of non-specific protein binding with Rodent Block M (Biocare Medical, Concord, CA). Slides were then incubated with pro-SPC primary antibody (Millipore ab3786), washed, and incubated with Rabbit-on-Rodent-HRP Polymer (Biocare Medical) prior to developing with DAB Chromogen (Biocare Medical) and counterstaining with Hematoxylin (Biocare Medical). Quantitation was performed by identifying 10 non-adjacent alveoli per field of view and counting the number of DAB-positive cells directly adjacent to the alveolar space. Six fields of view were imaged per mouse.

Two-color staining of pro-SPC and Cyclooxygenase 2 (COX2) in tissue sections was performed by immunofluorescence. De-paraffinization, peroxidase blocking, and antigen retrieval were performed as described. Non-specific protein blocking was done using 5% donkey serum in PBS followed by incubation of pro-SPC primary antibody (Millipore ab3786) in 3% donkey serum. A donkey anti-rabbit secondary antibody (Alexafluor 488; Invitrogen, Eugene, OR) was applied, sections were washed, and again blocked in 5% donkey serum prior to incubation with the second COX2 primary antibody (Novus Biologicals NB100-868, Littleton, CO) in 3% donkey serum

in PBS. This was followed by washing and application of the donkey anti-goat secondary antibody (Alexafluor 546; Invitrogen) and DAPI nucleic acid stain (Invitrogen). Four fields of view were imaged per sample using the Nuance multispectral imaging package (Elmer Perkins, Hopkinton, MA). Quantitation of SPC, COX2, and dual-stained (SPC +COX2) cells was performed manually, and the total number of DAPI positive cells was determined using the analyze particles function in Image J processing software (27).

RILI and collagen accumulation was verified at 24 weeks and later after irradiation by Gomori trichrome (VWR International Co., Radnor, PA) staining. Lung sections were examined by light microscopy, and images were acquired with an Olympus BX40 microscope (Olympus Imaging America Inc., Center Valley, PA). Fibrosis assessment was made using the modified Ashcroft scoring method as described by Hubner et. al. (28).

Collection of CD326+ Cells for RNA seq and qPCR

To rapidly isolate RNA from 12.5 Gy and non-irradiated tissue for sequencing, we developed a technique of rapidly isolating pulmonary epithelia based on the expression of the epithelial cell-adhesion molecule (EpCam) CD326 (Fig. 1). To isolate CD326+ epithelium from whole lung-tissue digest, cells were pelleted and resuspended in microbead buffer (PBS, 0.5% BSA, and 2 mM EDTA) plus CD45 magnetic microbeads (Miltenyi Biotech #130 052 301, Auburn, CA) per manufacturer's instructions to remove the CD45+ fraction of cells from the lung homogenate. This CD45-depleted population of cells was then recounted, pelleted, and resuspended in bead buffer plus CD326 microbeads (Miltenyi Biotech #130 105 958). Again, cells were washed in buffer solution, pelleted, and resuspended in 500 μl fresh buffer prior to a second magnetic separation using a Miltenyi LS column. Unbound CD326 negative cells were washed from the column, and CD326+ cells trapped within the column were flushed from the column and collected.

BEACH ET AL.

Cells were pelleted, washed, and transferred into 600µl RLT Lysis buffer (Qaigen, Hilden, Germany) and stored at –80°C until processing for RNA isolation. All RNA isolation, quality-control analysis, and low-input RNA sequencing procedures were performed by the University of Rochester Genomics Research Center.

Validation of CD326 Isolation by Immunocytochemistry and Flow Cytometry

Immunocytochemistry. Approximately 10^5 cells were resuspended in PBS and spun onto VWR SuperFrost Plus microscope slides (Radnor, PA), fixed in 3% paraformaldehyde, and incubated with either pro-SPC (Millipore ab3786, Burlington, MA) or CCSP separately (Abcam 40873, Cambridge, MA) followed by washing and incubation with the secondary Alexafluor 488 goat anti-rabbit antibody (Life Technologies A11008, Carlsbad, CA), re-washed, and incubated with DAPI (Molecular Probes D3571, Carlsbad, CA) prior to cover slipping. Quantitation was performed manually.

Flow cytometry. Approximately 10^6 of freshly isolated cells were transferred into staining buffer (PBS + 10%FBS), and nonspecific antibody binding was blocked using anti-mouse CD16/CD32 Fc block (BD Biosciences 553142, San Diego, CA) prior to surface staining with PerCP-Cy 5.5 rat anti-mouse EpCam (BioLegend 118220, San Diego, CA), Pacific Blue anti-mouse CD31 (BioLegend 102422), and PE anti-mouse CD45 (BioLegend 103106) antibodies. After surface staining, cells were washed and stained with LIVE/DEAD far red fixable dead cell stain (Life Technologies L34973) and resuspended in 2.5% phosphate buffered formalin (Fisher Scientific). Single-color compensation standards (positive controls) were created with Simply Cellular anti-mouse compensation standard (Bangs Laboratories, Fishers, IN). Samples were run on an 18-parameter LSRII flow cytometer (BD Biosciences), and data were analyzed using FlowJo (FlowJo, Ashland, OR).

qPCR Methods and Primers

Relative quantitation of gene expression was determined by comparison to the housekeeping gene GAPDH (Life Technologies, Mm99999915_g1) using the Taqman gene expression assay (Applied Biosystems, Carlsbad, CA) according to manufacturer's recommended protocol. The relative abundance of Cd200 (Mm00487740_m1) and Ptgs2 (COX2) (Mm03294838_g1) was compared in isolated CD326 mRNA, thus indicating the relative expression within the epithelial population of cells, while Sftpc (SPC) (Mm00488144) abundance was quantified by comparison to RNA isolated from whole lung tissue. RNA from five animals per time point and treatment group (n = 5) were examined for these experiments.

Low-input RNA Sequencing of CD326 Samples

Low-input RNA sequencing of epithelial samples requiring a minimum of 1ng mRNA was performed in identical fashion as that described for whole lung tissue samples (8). RNA concentrations were normalized, and 3–5 mice per time point and treatment group were pooled for low-input RNA seq analysis (N = 1) using the Illumina HiSeq 2500 Sequencer (Illumina, San Diego, CA). Differential expression of transcripts between irradiated and non-irradiated epithelial cells isolated from whole lung tissue was compared across time points. RNA sequencing data was trimmed and quality-controlled through the use of Trimmomatic 0.32 and fastQC software applications (29), mapped using star 2.4.2a mouse genome, and aligned to the GENECODE M6 gene annotation library prior to comparing differential expressions of transcripts between irradiated and non-irradiated tissue using cuffdiff2 (30).

Experimental Determination of CD326 Genes Involved in RIPF

We compiled a list of genes expressed across all time points, representing a list of genes experimentally determined to be differentially expressed in pulmonary epithelia during the progression of RIPF. From this list, we interrogated RNA-sequencing results using the predicted drivers function of Ingenuity Pathway Analysis (IPA) software (Qiagen) and selected for outcomes of cell death, inflammation of the lung, lung injury, fibrogenesis, and inflammatory response based on experimentally observed gene transcripts with a $\log_2$ fold change of greater than ± 0.25 across all time points. This identified transcripts predicted to drive the previously mentioned responses, which were then compared to their experimentally determined differential expression values. This method identified several transcripts as persistently decreased in abundance compared to non-irradiated controls across all time points examined, and we attempted to further validate these results by immunohistochemistry and/or qPCR.

Additionally, changes in the relative abundance of a number of gene transcripts known to be associated with inflammation and fibrosis were compared to isolated epithelia and whole lung tissue in irradiated and non-irradiated conditions, which identified several transcripts more abundant in epithelia compared to other cells in the lung (Fig. 2A and B). We also compared irradiated epithelia and non-irradiated epithelia (Fig. 2C). These results were displayed as heatmaps created with the Multi Experiment Viewer (MeV) software application version 4.9.0. (31).

Statistical Analysis

Results were considered statistically significant at P ≤ 0.05. Histology results for pro-SPC and COX2 expression were compared by one-way ANOVA and Tukey after hoc analysis using GraphPad Prism, version 8.0.0 for Windows (San Diego, CA). qPCR comparisons of means were conducted by one-way ANOVA and a preselected contrast of means using R statistical software, version 3.5.2 (32).

RESULTS

Validation of CD326 Isolation

Flow-cytometry experiments indicated that 91% of all cells isolated by magnetic microbead enrichment were EpCam (CD326) positive with 80% of the total cells identified as CD45 and CD31 negative, indicating only a small number of cells that displayed markers of immune or endothelial cells that were likely doublets. Cytospin preparations of isolated CD326+ cells revealed this population to be largely pro-SPC-positive, with the ratio of pro-SPC to CCSP-positive cells to be 2.4:1, respectively. It is also likely that a small proportion of these cells are pro-SPC and CCSP-positive BASCs residing at the bronchi-alveolar junction (14).

The use of magnetic microbeads allowed for a rapid isolation of cells in to obtain epithelial RNA of sufficient quality for RNA sequencing, which we were unable to reliably obtain using flow sorting methods such as that described by Hasegawa et. al. (33). As a result, immunohistochemistry was required to verify reduced expression of COX2 in AEC2 cells, and further experimentation is needed to determine if the loss of CD200 expression is limited to AEC2 cells.

Decreased Abundance of Transcripts Associated with Fibrosis and Immune Response

We examined patterns of transcript abundance over time for Tgfβ, Tnfα, Il-6, and Il-1α, which have been shown to

be expressed by club cells and AEC2 in vivo (*34, 35*). However, at the transcriptional level, Tnf-α, Il-6, and Il-1α were far less abundant ($\geq$–2 log$_2$ fold change or undetected) in the irradiated and non-treated comparisons of epithelial cells to whole lung tissue (Fig. 2A and B) and were not reliably detected at multiple time points in the comparison of irradiated and non-irradiated epithelia. Tgf-β gene transcripts also appeared far less abundant within the CD326 population as compared to whole tissue in both irradiated and non-irradiated conditions (Fig. 2A and B). This was also true for the comparison between irradiated and non-irradiated epithelia (Fig. 2C), with a log$_2$ fold change greater than –2 at all times examined. This indicated a greater abundance of Tgf-β transcripts in other cell types, such as macrophages or monocytes, present in the whole lung comparison, and a greater abundance in non-irradiated epithelia as compared to irradiated tissue.

Gene transcripts that indicated the greatest fold change in irradiated CD326 as compared to non-irradiated controls were examined by IPA and identified several potential drivers of inflammation, fibrosis, and lung injury. Interrogation of the sequencing data set for additional transcripts associated with those identified by IPA or known to play a role in lung inflammation and/or pulmonary fibrosis (Fig. 2A–C) were included for this analysis.

From the heatmaps comparing transcriptional abundance in CD326 as compared to whole lung tissue, we identified a transcriptional signature more abundant in the CD326 than in whole tissue, particularly in the non-irradiated comparison (Fig. 2B). These crucial genes contribute to the maintenance of homeostasis under steady-state conditions, the expression of which appears to be altered in response to radiation. We identified Cd200, Csf1, Csf2, Cxcl1, Cxcl15, Ptgs1, Ptgs2, Fgf1, Pdgfa, and Vegfa as part of the transcriptional repertoire of non-irradiated epithelium in whole lung tissue, generally displaying a log$_2$ fold increase from 1 to 3 for the duration of the experiment. Of these, CD200, Csf1, Csf2, Cxcl15, Ptgs1, Ptgs2, and Vegfa are all generally decreased in abundance after irradiation, particularly when log$_2$ fold change values were averaged for individual transcripts across all time points (Fig. 2D); therefore, we attempted further validation in tissue sections and by qPCR. No statistical comparisons of RNA sequencing data were made.

Pro-SPC Expressing Cells Decrease Significantly in the Progression of RILI

The numbers of pro-SPC-expressing type-2 AECs were quantified in lung tissue as a number of SPC-positive cells per alveolus (Fig. 3A) and as a percent of total cells per field of view (Fig. 3B). The results of both methods of quantitation were similar at the dose of 12.5 Gy. As detected by brightfield microscopy, the number of AEC2 cells per alveolus is significantly decreased at 4 weeks postirradiation as compared to similar aged controls (Fig.

3A). A second significant decrease occurred at 32 weeks, indicating a somewhat delayed cell death after radiation exposure within this cell type. In fact, the number of pro-SPC-positive cells are relatively unchanged from non-irradiated controls at 24 h and 1-week postirradiation. Fluorescence microscopy relying on the same pro-SPC antibody also indicates a significant decrease in the number of SPC-positive cells at 16, 24, and 32 weeks (Fig. 3B). It is likely that these statistics differ slightly due to the method of quantitation of SPC as a percent of total cells, which was necessary because the alveolar structure is not visible in fluorescent images. Nonetheless, both methods of quantitation indicate that the decline in the number of SPC-positive cells occurs in delayed fashion.

Importantly, a significant loss of SPC-expressing cells was not observed at any time in mice that were exposed to a lower dose of 10 Gy (Fig. 3B). At this dose, there was no observable mortality due to RIPF, although histology did indicate the presence of minor inflammation and minimal fibrosis as evident in H&E and Trichrome-stained lung tissue sections as previously published(*26*), and shown in Fig. 6A. Statistical comparison indicates a significantly greater number of SPC-expressing cells present in tissue sections of 10-Gy animals as compared to those exposed to 12.5 Gy at 24 and 32 weeks.

Pulmonary Epithelia (AEC2 and Club Cells) are the Primary Cell Types in the Lung that Express COX2

We sought to determine if AEC2 cells express the PGE$_2$ producing enzyme, COX2. Dual staining of lung tissue sections from both irradiated (10 and 12.5 Gy) and non-irradiated animals indicated that the majority of COX2-expressing cells are epithelia (Fig. 4A and D). In non-irradiated animals, over 92% of SPC-positive cells expressed COX2; at 10 Gy, this percentage decreased only slightly (89%); and these numbers were not significantly different from those of mice exposed to 12.5 Gy examined at any point in the course of these experiments, except at 24 weeks after 12.5-Gy irradiation (Fig. 4A). Observations of club cells lining the airways revealed these cells to be COX2-positive in all treatment conditions, indicating that the great majority of cells in lung tissue expressing COX2 appear to be of the epithelial type. Regardless of the treatment condition, only a small number of COX2-positive, pro-SPC-negative, non-airway cells were observed in any of the tissue sections, and because of this, the number of COX2-expressing cells closely reflects the number of pro-SPC-positive cells across all samples.

COX2 Expression Decreases Significantly as the Number of Pro-SPC-Expressing Cells Decreases

Because the number of COX2-positive cells closely follows the number of SPC-expressing cells in 12.5-Gy irradiated mice (Figs. 3B, 4B and D), a similar pattern of reduced COX2 expression over time is observed. At 12.5
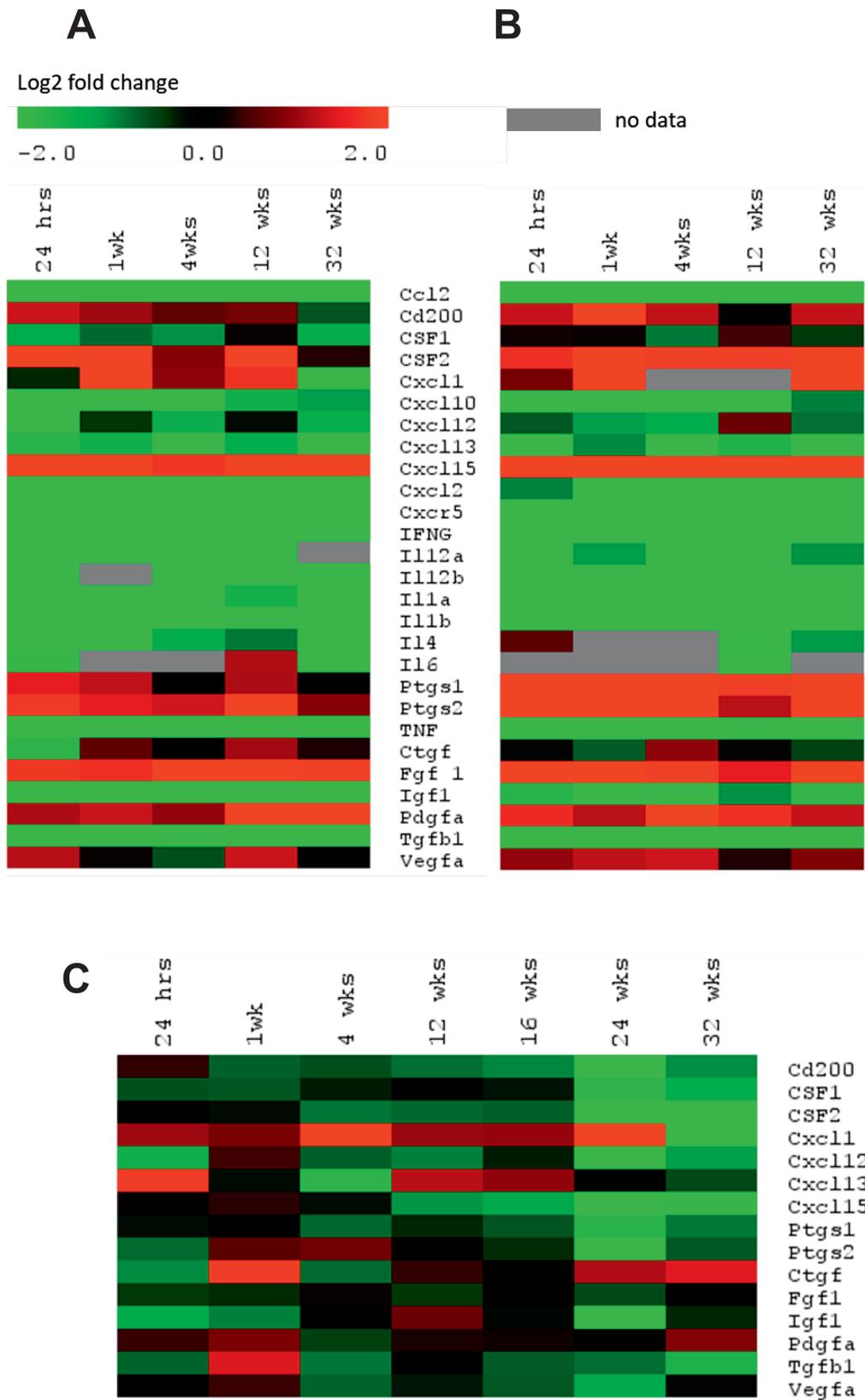
FIG. 2A–C. Transcriptional changes in growth factor and inflammatory response genes. Panel A: CD326 vs. whole lung (12.5 Gy). Comparisons between epithelia and whole lung tissue in irradiated animals. Panel B: CD326 vs. whole lung (0 Gy). Epithelia and whole lung tissue in non-irradiated animals indicate an increased transcript abundance within the epithelial population (red). Panel C: CD326 12.5 Gy vs. 0 Gy. Comparison between irradiated and non-irradiated epithelia indicates decreased transcriptional abundance (green) in the irradiated condition.
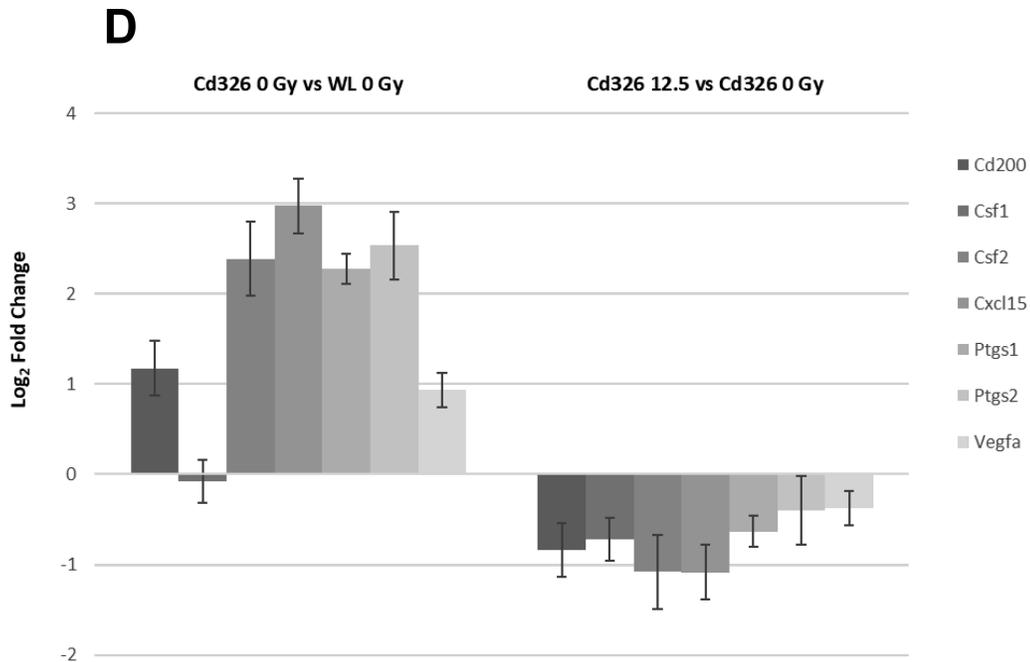
FIG. 2D. Comparison of cd326 mean transcript abundance over time in non-irradiated and irradiated conditions. Mean transcriptional abundance over time for selected gene transcripts as measured by RNA seq. Error bars represent the standard deviation of the mean.

Gy, fewer COX2-expressing cells are present at 4 and 12 weeks (Fig. 4B). At 16 and 24 weeks, this reduction is statistically significant, and fewer COX2-expressing cells are seen for the remainder of the experiment.

In the 10-Gy irradiated mice with no RIPF-associated mortality, expression of COX2 is maintained at higher levels than in animals exposed to 12.5 Gy, particularly at 24 weeks postirradiation and the levels are not significantly reduced compared to similar aged controls at any point. In fact, during both early and late response periods, COX2

expression is nearly identical to controls, and it is significantly greater than in mice exposed to 12.5 Gy at 24 weeks (Fig. 4B and D).

Pro-SPC and COX2 Dual Staining of Lung Tissue Sections Indicates a Reduction of Functional AEC2 Cells

Similar to observations of SPC and COX2 in tissue sections, the number of dual-labeled cells is not significantly different during the period immediately after irradiation; however, at 4 weeks, there is a notable decline
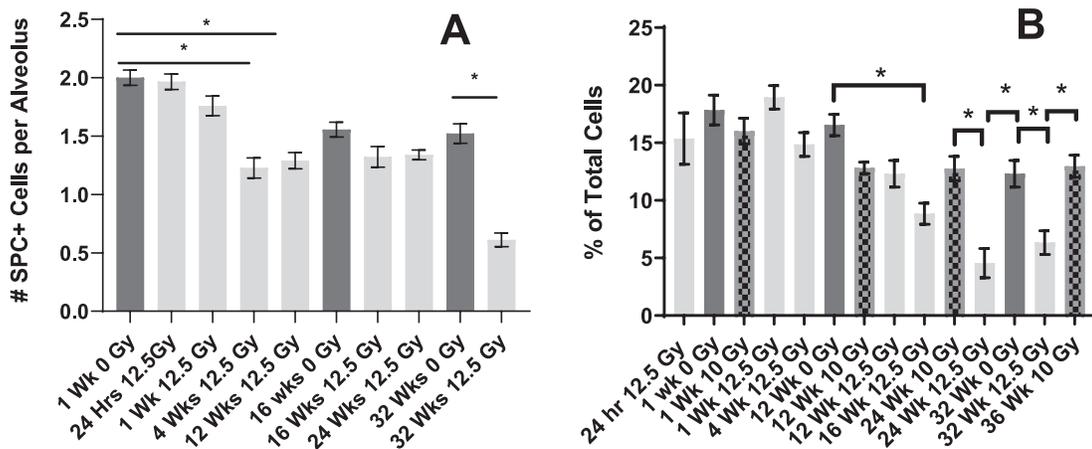
FIG. 3. Panel A: SPC expression in lung tissue sections. Pro-SPC positive cells per alveolus: A significant decrease in the number of pro-SPC expressing cells is observed at 4 weeks postirradiation, which is maintained at 12 weeks and further decreased at 32 weeks. *$P \leq 0.05$ by one-way ANOVA and Tukey after hoc analysis (N = 3 for each time point). Panel B: Percent of total cells expressing pro-SPC: A significant decrease in the number of pro-SPC-expressing cells as a percent of total cells is observed at 16 weeks postirradiation at 12.5 Gy, with further decreases at 24 and 32 weeks. No significant difference between the number of pro-SPC-expressing cells was observed between the 10 Gy exposure and controls. At 24 and 32 weeks, pro-SPC expression was significantly higher in 0 and 10 Gy groups as compared to 12.5 Gy groups. *$P \leq 0.05$ by one-way ANOVA and Tukey after hoc analysis (N = 3 for 0 and 12.5 Gy groups, N = 2 for 10 Gy).
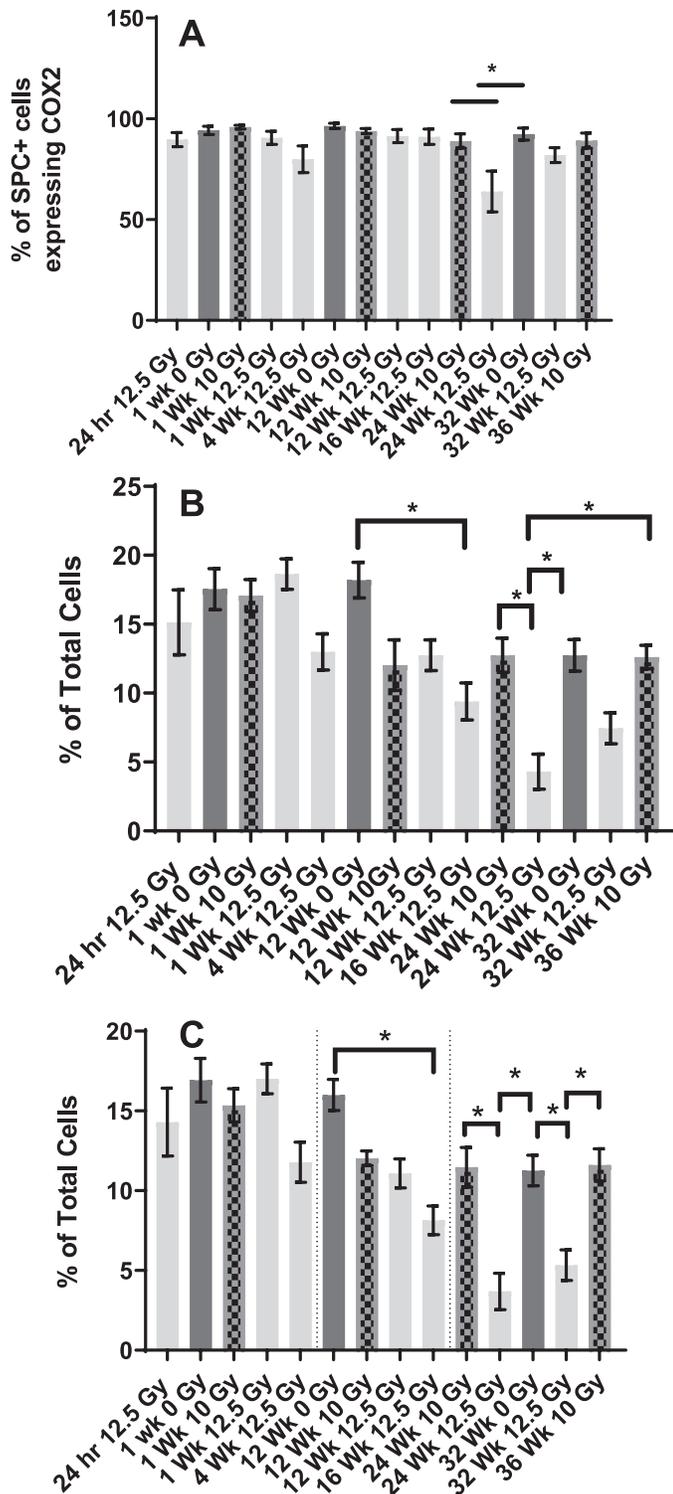
FIG. 4. SPC and COX2 expression in lung tissue sections. Panel A: Percent of pro-SPC-expressing cells expressing COX2. Nearly all pro-SPC-positive AEC2 cells express COX2, except within highly cellularized regions detected within 12.5-Gy irradiated animals at 24 weeks. Panel B: Percent of total cells expressing COX2. A significant decrease in the numbers of COX2-positive cells was observed at 16 and 24 weeks in the 12.5-Gy exposure group. In contrast, at 10 Gy, no significant reduction in COX 2 expression as compared to controls was observed. At 24 weeks, COX2 expression was lower within the 12.5-Gy group as compared to the 0- and 10-Gy-exposed animals of

in the numbers of dual-labeled cells as compared to controls (Fig. 4C), which reflects the changes observed in the number of epithelial cells (Fig. 3A). This decline in dual-labeled cells continues during the progression of injury, becomes statistically significant at 16 weeks, and remains significantly reduced at 24 and 32 weeks. Interestingly, images of fibrotic lesions (Fig. 4D, 12.5 Gy at 24 weeks) reveal a nearly complete lack of SPC, COX2, or dual-labeled cells, indicating that both surfactant production and the antifibrotic mediator PGE_2 are likely markedly reduced within these fibrotic lesions.

In mice exposed to a lower dose of 10 Gy, this significant reduction of dual-labeled cells does not occur at any time examined. A slight reduction in the number of dual-labeled cells (3%) occurs at 12 weeks postirradiation (Fig. 4C and D); however, this does not progress further and, in fact, the number of dual-labeled cells remains constant for the duration of the experiment. The number of dual-labeled cells is significantly higher in the 10-Gy group as compared to the 12.5-Gy exposed animals during the later time points.

SPC Transcript Abundance Decreases in Irradiated Whole Lung Tissue Over Time

Relative quantitation of Spc transcript abundance in whole lung tissue digest indicates an immediate response to radiation treatment, as transcript abundance increases compared to age-matched controls at 24 h and 1-week postirradiation (Fig. 5), although these increases are not statistically significant due to large sample variance within several time points. However, at 12, 24, and 32 weeks, these transcripts are notably reduced in abundance in the irradiated animals. In particular, at 12 and 24 weeks, the irradiated groups are significantly lower than at the 24-h 0 Gy control. This decreased abundance of Spc transcripts over time is similar to pro-SPC quantitation by histology (Fig. 3A and B), which indicates a significant decline in the numbers of pro-SPC expressing cells as early as 4 weeks postirradiation. Cox2 (Ptgs2) transcript abundance decreases in irradiated (CD326+) epithelial cells.

←

similar age. Panel C: Percent of total cells dual labeled for pro-SPC and COX2. A significant decrease in the number of dual positive cells as a percent of total cells was observed at 16 weeks postirradiation after 12.5 Gy, with a further decrease at 24 weeks, which was similarly maintained at 32 weeks. In contrast, no significant difference between the number of dual-labeled cells was observed between the 10-Gy exposure and controls. At 24 and 32 weeks, the number of dual-labeled cells was significantly higher in the 10-Gy group as compared to 12.5 Gy. *$P \leq 0.05$ by one-way ANOVA, and Tukey after hoc analysis. Panel D: Representative images showing expression of pro-SPC (green) and COX-2 (red) co-localized (yellow) to DAPI (blue) stained nuclei. Co-localization of pro-SPC, COX2, and DAPI (yellow) expression is reduced in 10- and 12-Gy irradiated animals compared to age matched controls, and noticeably reduced in 12.5 Gy irradiated lungs at 24 and 32 weeks compared to 32-week controls.
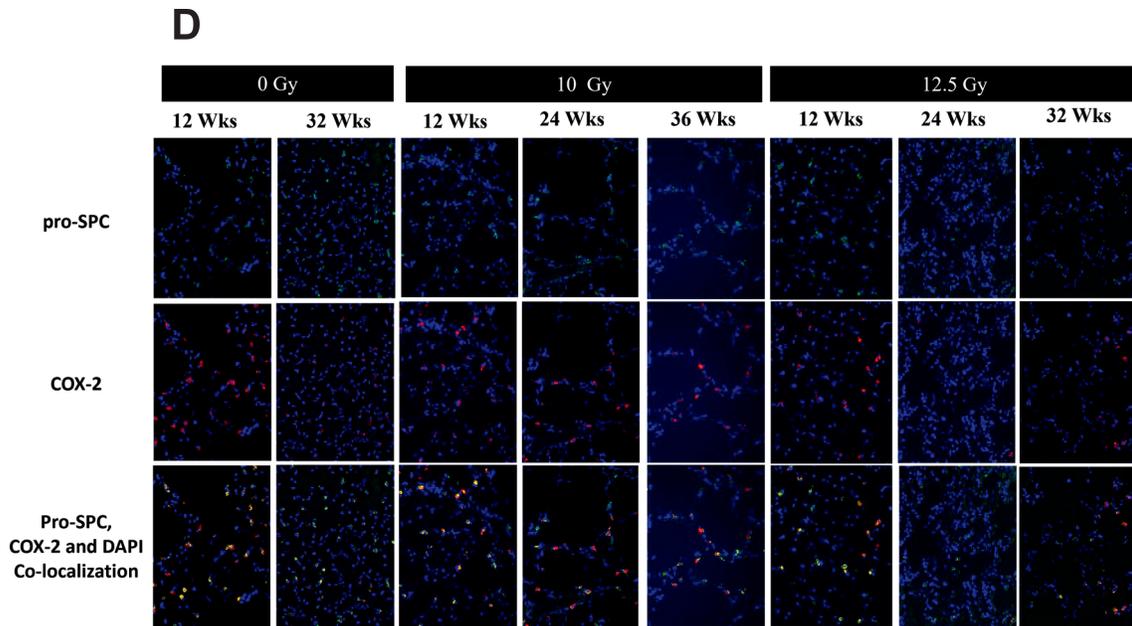
FIG. 4. Continued.

To interrogate changes within epithelial cells and further validate the results of our RNA sequencing of these cells, we performed relative quantitation of both Cd200 and Ptgs2 using RNA isolated from our CD326-enriched cell population. By examining this cell type, we can interrogate changes within the epithelial cells surviving irradiation or newly generated after to gain insight on the relative functionality of the remaining epithelia.

Cox2 (Ptgs2) abundance increased sharply immediately after irradiation at 24 h (Fig. 5B), a response that is consistent with previous reports (36). However, at the following time points, abundance is reduced compared to age-matched controls, which supports the findings of RNA sequencing (Fig. 2D) and examination of tissue sections (Fig. 4B). Most notably, Cox2 transcript abundance is significantly reduced at 12, 24, and 32 weeks, similar to COX2 protein expression in tissue sections.

Cd200 Transcript Abundance Decreases in Irradiated (CD326+) Epithelial Cells

At 24 h postirradiation, a statistically significant increase in Cd200 expression was observed (Fig. 5C). However, by 1 week, the relative expression of this transcript had returned to baseline values and then continued to decline for up to 24 weeks postirradiation. A statistically significant decrease in transcript abundance compared to similar aged controls was detected at 4 weeks postirradiation, which was maintained through weeks 12 and 16.

Verification of Fibrotic Lesions at 12.5 Gy

Trichrome stained lung tissue sections at 24 weeks indicate the presence of fibrotic lesions in the 12.5 Gy irradiated lungs, which are absent in controls and animals irradiated at 10 Gy (Fig. 6A). Fibrosis scores generated using the modified Ashcroft soring method (Fig. 6B), which assesses changes to the alveolar septa and presence of fibrotic masses, further support observations increased cellularity and collagen accumulation at 12.5 Gy, 24 weeks postirradiation, but not in 10 Gy irradiated animals at 24- or 36-weeks postirradiation.

DISCUSSION

AECs play a crucial role in maintaining homeostatic conditions in the lung. Because of this, we sought to quantify the numbers of SPC-expressing cells over time, comparing the response to WTLI at a dose known to be sufficient to result in fibrosis (12.5 Gy) to a lower dose (10 Gy) in which lethal RIPF did not develop.

SPC Expression Decreases after Irradiation

We elected to quantify pro-SPC expression of AEC2s per alveolus in animals receiving 12.5 Gy to reduce the influence of increased cellularity due to radiation pneumonitis on our results. In the untreated animals, the majority of alveoli contained more than one AEC2 with between 1.5 and 2 AEC2s per alveolus (Fig. 3A). However, in the irradiated animals, this number was significantly reduced in similarly aged controls to an average of roughly 1 cell per alveolus as early as 4 and 12 weeks postirradiation, with an even greater reduction occurring at 32 weeks.

Additional quantitation of pro-SPC expression in tissue sections was performed as SPC expression as a percent of total cells in mice exposed to either 12.5 Gy or 10 Gy (Fig.
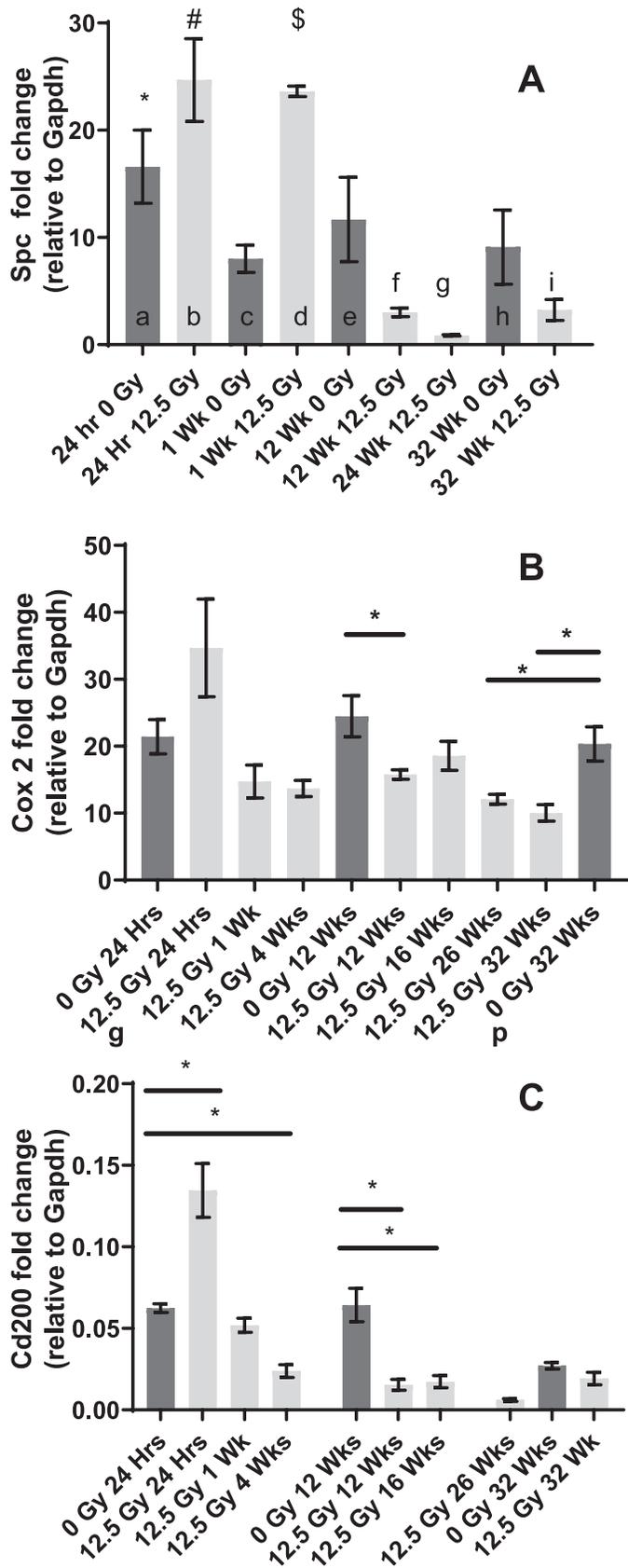
3B). This method of quantitation allows for examination of SPC within fibrotic or inflammatory lesions that occur at the margins of irradiated tissue with the understanding that this method is influenced to a degree by the influx of immune cells resulting from RILI. Limitations aside, the results of this method were similar to alveolar quantitation in the 12.5-Gy irradiated animals, but surprisingly, the 10-Gy irradiated animals (which did not develop lethal RIPF) were similar to controls. However, in the 12.5-Gy group, a significant reduction in SPC expression was observed at 16, 24, and 32 weeks postirradiation. Furthermore, at 24 and 32 weeks, the numbers of SPC-expressing cells were significantly lower for the 12.5-Gy group as compared to the 10-Gy non-fibrotic group, suggesting an association between the SPC loss of expression and mortality due to fibrosis.

To further validate the histological findings of SPC abundance in tissue sections, qPCR was performed comparing RNA obtained from whole lung tissue. At 24 h and 1 week postirradiation, Spc-transcript abundance increased in irradiated tissue (Fig. 5A), which is consistent with findings showing increased surfactant in bronchoalveolar lavage fluid of irradiated mice up to one month after irradiation (37). However, by 12 and 24 weeks postirradiation, transcript values were reduced significantly compared to the 24-h, 0-Gy control animals, this reduction persisted for the duration of the experiment and was consistent with the loss of pro-SPC protein expression.

The simplest explanation for reduced SPC expression within tissue sections and RNA isolated from whole lung tissue is the loss of SPC-expressing AEC2s, which appears in delayed fashion. Indeed, significantly decreased expression of pro-SPC occurs during the period of immediate injury as early as 4 weeks and at 12 or 16 weeks, suggesting a loss of cells in the progression of injury supporting the notion that a loss of epithelial cells is sufficient to induce fibrosis. However, a number of limitations must be considered before accepting this hypothesis; most importantly, additional indicators of AEC2 cells were not examined in tissue sections, and no direct measurement of cell death (such as apoptosis), cellular senescence, or DNA damage (γ-H2AX) was recorded within this population. It may be possible that, rather than dying, AECs become functionally altered after WTLI, remain in the tissue, and no longer display the canonical indicators of this cell type. Perhaps it is a combination of AEC2 cell death and loss of functions crucial to maintaining homeostasis that contribute to the failure of lung tissue to properly repair after RILI.

FIG. 5. Transcript abundance in whole lung tissue and CD326+ cells. Panel A: Sftpc transcript (Spc) abundance in whole lung tissue. Spc was significantly reduced at 12, 25, and 32 weeks as compared to 24-h non-irradiated controls. Panel B: Relative Cox2 (Ptgs2) transcript abundance in CD326 cells. Cox2 was significantly decreased at 12 weeks and further reduced in irradiated animals at 24 and 32 weeks. Panel C: Relative Cd200 transcript abundance in CD326 cells. Cd200 was significantly decreased at 4 weeks, and this decrease was maintained at 12 and 16 weeks. *P $\leq$ 0.05 by one-way ANOVA and pre-selected contrast of means.

A

32 Weeks 0 Gy   24 Weeks 12.5 Gy   24 Weeks 10 Gy   32 Weeks 12.5 Gy   36 Weeks 10 Gy

B
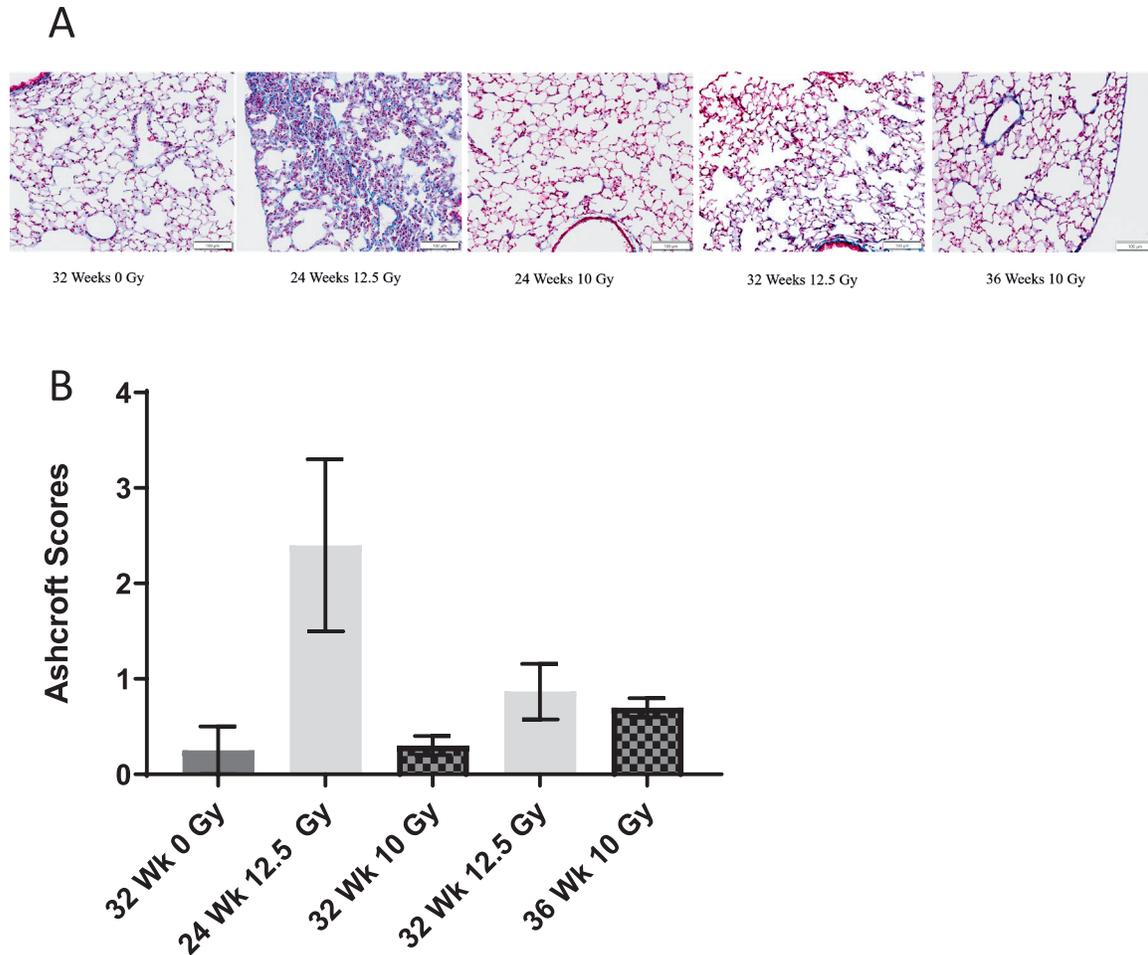
FIG. 6. Trichome staining and modified Ashcroft scores of controls and irradiated lungs at 24 weeks and later after irradiation. Panel A: Trichome staining of representative lung tissue sections reveal areas of increased collagen deposition and in lungs irradiated at 24 weeks after 12.5 Gy irradiation, which are notably absent in 10 Gy irradiated lungs at 24 and 36 weeks. Panel B: Modified Ashcroft scores of controls and irradiated lungs at 24 weeks and later.

Epithelial Cells May Allow Macrophage Activation in RILI as Result of Decreased CD200 Expression

Pulmonary epithelia regulate alveolar macrophage function to maintain immunologic homeostasis via the expression of CD200 (*19*). At the transcriptional level, Cd200 is consistently present in CD326 cells under steady-state conditions (Fig. 5C). Yet after irradiation, this transcript is significantly reduced by 4 weeks, which may allow for the inappropriate activation of infiltrating immune cells long after the initial radiation injury. In fact, previous experiments in this same WTLI model have demonstrated increased numbers of Ly6C expressing pro-inflammatory alveolar macrophages at the 12.5 Gy dose (*12*). It is possible that via the decreased expression of CD200, epithelial cells are not actively promoting inflammation; rather, they passively permit the activation of immune cells recruited into the lung. Because Cd200 transcript abundance was measured within surviving epithelia this effect may be further exacerbated by the possible loss of AEC2 or club cells, as indicated in our other experiments (Fig. 3A and B).

Thus, it is likely that fewer CD200-expressing cells are present in the irradiated lung, and those cells that remain may no longer function effectively to suppress inflammation and restore resting homeostatic function within the macrophage population.

Epithelial Cells May Allow Fibroblast Activation in RILI as Result of Decreased COX Expression

Because we were able to compare tissue obtained from animals exposed to 12.5 and 10 Gy WTLI, there were no significant differences in any of our measures between the 10-Gy and non-irradiated groups (Fig. 4B). Our dual-staining experiments show that AEC2s (Fig. 4A) and club cells (not shown) constitutively express COX2 in steady-state and irradiated conditions with little or no expression found in other cell types present. The only exception to this occurred within the 12.5-Gy irradiated animals at 24 weeks postirradiation (Fig. 4A), where pro-SPC-positive cells were absent from highly cellularized lesions and few COX2 expressing cells were detected.

As the number of pro-SPC-expressing cells decline, COX2 expression declined in identical fashion in both the 10-Gy and 12.5-Gy groups (Fig. 4C). At 10 Gy, a modest decline in dual positive (pro-SPC, COX2) cells occurred at 12 weeks postirradiation (5% of total cells) and did not progress further. However, at 12.5 Gy, a more pronounced decline began at 4 weeks postirradiation and continued over time. By 16 weeks, this loss of COX2-expressing AEC2s was statistically significant, and an even greater reduction of cell numbers was observed at 24 and 32 weeks postirradiation. Again, these results indicate a loss of COX2-expressing AEC2s cells, which is maintained for the duration of the experiment. The loss of COX2 expression, which appears to be directly correlated to the number of pro-SPC-expressing cells, reveals yet another possible mechanism by which the loss of epithelial cells can passively contribute to the onset of RIPF. This mechanism supports the notion that a loss of epithelial cells is sufficient to induce fibrosis and appears to be a failure of the epithelium to suppress fibroblast activity due to the reduced production of PGE_2, rather than actively promoting pro-fibrotic actions of fibroblasts through the release of mitogens or other means.

The interrogation of CD326 mRNA by qPCR also indicates a significant reduction in Ptgs2 (COX2) transcripts at 12, 24, and 32 weeks (Fig. 5B), indicating that the remaining epithelia are potentially diminished in their capacity to express the COX2 enzyme, a key player in the synthesis of PGE_2. It appears that the decreased abundance of Cox2 transcript after irradiation is not entirely caused by a loss of AEC2s, as this change is occurring within the CD326 population. This finding raises the distinct possibility that reduced expression of COX2 within the remaining CD326 population is further exacerbated by the loss of AEC2 cells.

Contrary to our initial hypothesis, the findings of the experiments indicate that epithelial cells do not actively promote inflammation or fibrogenesis through the production of pro-inflammatory or pro-fibrotic agents (Fig. 2C). Instead, the capacity to prevent myeloid cell activation through the expression of CD200 is reduced, and this inappropriate macrophage activation can allow for further inflammation and possible production of reactive oxygen species. Similarly, epithelial regulation and suppression of fibroblast chemotaxis, proliferation, and other activities that allow for extracellular matrix accumulation via the production of PGE_2 may be significantly reduced in the weeks after irradiation. In addition, both club cells and AEC2 appear to decrease in number over time, leaving a smaller pool of cells to maintain homeostatic conditions through the suppression of inflammation and fibroblast activation.

In the 10-Gy tissue sections, we did not observe any significant decrease in pro-SPC or COX2 expression, contrary to our observations of mice exposed to the higher dose of 12.5 Gy. This finding supports the notion that RIPF is a deterministic effect of radiation exposure, and the threshold for development may lie somewhere within the range of 10–12.5 Gy in the WTLI/C57BL/6J model.

The data presented here has important new implications regarding the loss of epithelial regulation of immune and fibroblast populations, which should be considered in context with other events known to occur in RILI, such as chronic oxidative stress and cellular senescence for the development of treatment strategies to mitigate RILI/RIPF after the initial exposure to radiation. Perhaps senescence within the lung epithelium results in a loss of function for certain homeostatic mechanisms. Previously we reported significant increases in p21 transcript abundance and senescence associated beta galactosidase staining in whole lung tissues of these same animals (9), and others have specifically reported increases in AEC2 senescence in response to whole thorax irradiation (6). Indeed, there is mounting evidence that epithelial senescence does play a role in the development of RIPF (38). Although the data presented here indicates important changes within the CD326+ population of cells with respect to the development and progression of RILI, further experimentation is needed to determine the mechanism(s) responsible.

At 10 Gy, there appeared to be only a minor reduction in the number of SPC-expressing cells, and these mice failed to develop lethal lung injury. It appears that protection of resident epithelial cells at the time of irradiation, perhaps through the administration of an antioxidant or free radical scavenger, may offer a potential strategy to prevent delayed lung injury. Indeed, this approach has been shown to be effective in clinical trials; patients receiving radio-chemo-therapy for non-small-cell lung cancer had significantly reduced incidence of pneumonitis when given amifostine just prior to treatment (39, 40). Targeting senescence, specifically clearance of senescent cells using senolytic agents, may also have potential to treat RIPF. ABT-263 was demonstrated to selectively reduce the number senescent AEC2s in WTLI treated animals, which was associated with a reduction in RILI pathology scores (41). Lastly, short of preventing epithelial cell loss, replacement of epithelial mediators of inflammation or fibrogenesis, such as CD200 or PGE_2, may prove helpful in delaying or preventing the progression of injury if applied locally at the appropriate dose when functional epithelial cells are reduced in number. This type of replacement therapy would likely need to be provided over an extended duration, and further research is needed to determine the practicality and efficacy of this approach.

ACKNOWLEDGMENTS

REFERENCES

1. Sisson TH, Mendez M, Choi K, Subbotina N, Courey A, Cunningham A, et al. Targeted injury of type II alveolar epithelial cells induces pulmonary fibrosis. Am J Respir Crit Care Med 2010; 181:254-63.

2. Borensztajn K, Crestani B, Kolb M. Idiopathic pulmonary fibrosis: from epithelial injury to biomarkers–insights from the bench side. Respiration 2013; 86:441-52.

3. Camelo A, Dunmore R, Sleeman MA, Clarke DL. The epithelium in idiopathic pulmonary fibrosis: breaking the barrier. Front Pharmacol 2014; 4:173.

4. Corvol H, Flamein F, Epaud R, Clement A, Guillot L. Lung alveolar epithelium and interstitial lung disease. Int J Biochem Cell Biol 2009; 41:1643-51.

5. Cheresh P, Kim SJ, Tulasiram S, Kamp DW. Oxidative stress and pulmonary fibrosis. Biochim Biophys Acta 2013; 1832:1028-40.

6. Citrin DE, Shankavaram U, Horton JA, Shield W, Zhao S, Asano H, et al. Role of type II pneumocyte senescence in radiation-induced lung fibrosis. J Natl Cancer Inst 2013; 105:1474-84.

7. Perl AK, Riethmacher D, Whitsett JA. Conditional depletion of airway progenitor cells induces peribronchiolar fibrosis. Am J Respir Crit Care Med 2011; 183:511-21.

8. Beach TA, Johnston CJ, Groves AM, Williams JP, Finkelstein JN. Radiation induced pulmonary fibrosis as a model of progressive fibrosis: Contributions of DNA damage, inflammatory response and cellular senescence genes. Exp Lung Res 2017; 43:134-49.

9. Beach TA, Groves AM, Johnston CJ, Williams JP, Finkelstein JN. Recurrent DNA damage is associated with persistent injury in progressive radiation-induced pulmonary fibrosis. Int J Radiat Biol 2018; 94:1104-15.

10. Groves AM, Johnston CJ, Misra RS, Williams JP, Finkelstein JN. Effects of IL-4 on pulmonary fibrosis and the accumulation and phenotype of macrophage subpopulations following thoracic irradiation. Int J Radiat Biol 2016; 92:754-65.

11. Groves AM, Johnston CJ, Williams JP, Finkelstein JN. Role of Infiltrating Monocytes in the Development of Radiation-Induced Pulmonary Fibrosis. Radiat Res 2018; 189:300-11.

12. Groves AM, Johnston CJ, Misra RS, Williams JP, Finkelstein JN. Whole-Lung Irradiation Results in Pulmonary Macrophage Alterations that are Subpopulation and Strain Specific. Radiat Res 2015; 184:639-49.

13. Hogan BL, Barkauskas CE, Chapman HA, Epstein JA, Jain R, Hsia CC, et al. Repair and regeneration of the respiratory system: complexity, plasticity, and mechanisms of lung stem cell function. Cell Stem Cell 2014; 15:123-38.

14. Barkauskas CE, Cronce MJ, Rackley CR, Bowie EJ, Keene DR, Stripp BR, et al. Type 2 alveolar cells are stem cells in adult lung. J Clin Invest 2013; 123:3025-36.

15. Mason RJ. Biology of alveolar type II cells. Respirology 2006; 11 Suppl:S12-5.

16. Broeckaert F, Bernard A. Clara cell secretory protein (CC16): characteristics and perspectives as lung peripheral biomarker. Clin Exp Allergy 2000; 30:469-75.

17. Snelgrove RJ, Goulding J, Didierlaurent AM, Lyonga D, Vekaria S, Edwards L, et al. A critical function for CD200 in lung immune homeostasis and the severity of influenza infection. Nat Immunol 2008; 9:1074-83.

18. Bozyk PD, Moore BB. Prostaglandin E2 and the pathogenesis of pulmonary fibrosis. Am J Respir Cell Mol Biol 2011; 45:445-52.

19. Holt PG, Strickland DH. The CD200-CD200R axis in local control of lung inflammation. Nat Immunol 2008; 9:1011-3.

20. Lama V, Moore BB, Christensen P, Toews GB, Peters-Golden M. Prostaglandin E2 synthesis and suppression of fibroblast proliferation by alveolar epithelial cells is cyclooxygenase-2-dependent. Am J Respir Cell Mol Biol 2002; 27:752-8.

21. Kohyama T, Ertl RF, Valenti V, Spurzem J, Kawamoto M, Nakamura Y, et al. Prostaglandin E2 inhibits fibroblast chemotaxis. Am J Physiol Lung Cell Mol Physiol 2001; 281:L1257-63.

22. Bitterman PB, Wewers MD, Rennard SI, Adelberg S, Crystal RG. Modulation of alveolar macrophage-driven fibroblast proliferation by alternative macrophage mediators. J Clin Invest 1986; 77:700-8.

23. Epa AP, Thatcher TH, Pollock SJ, Wahl LA, Lyda E, Kottmann RM, et al. Normal Human Lung Epithelial Cells Inhibit Transforming Growth Factor-beta Induced Myofibroblast Differentiation via Prostaglandin E2. PLoS One 2015; 10:e0135266.

24. Huang S, Wettlaufer SH, Hogaboam C, Aronoff DM, Peters-Golden M. Prostaglandin E2 inhibits collagen expression and proliferation in patient-derived normal lung fibroblasts via E prostanoid 2 receptor and cAMP signaling. Am J Physiol Lung Cell Mol Physiol 2007; 292:L405-13.

25. Borok Z, Gillissen A, Buhl R, Hoyt RF, Hubbard RC, Ozaki T, et al. Augmentation of functional prostaglandin E levels on the respiratory epithelial surface by aerosol administration of prostaglandin E. Am Rev Respir Dis 1991; 144:1080-4.

26. Manning CM, Johnston CJ, Hernady E, Miller JN, Reed CK, Lawrence BP, et al. Exacerbation of lung radiation injury by viral infection: the role of Clara cells and Clara cell secretory protein. Radiat Res 2013; 179:617-29.

27. Schneider CA, Rasband WS, Eliceiri KW. NIH Image to ImageJ: 25 years of image analysis. Nat Methods 2012; 9:671-5.

28. Hübner R-H, Gitter W, Eddine El Mokhtari N, Mathiak M, Both M, Bolte H, et al. Standardized quantification of pulmonary fibrosis in histological samples. Biotechniques 2008; 44:507-17.

29. Bolger AM, Lohse M, Usadel B. Trimmomatic: a flexible trimmer for Illumina sequence data. Bioinformatics 2014; 30:2114-20.

30. Trapnell C, Hendrickson DG, Sauvageau M, Goff L, Rinn JL, Pachter L. Differential analysis of gene regulation at transcript resolution with RNA-seq. Nat Biotechnol 2013; 31:46-53.

31. Howe EA, Sinha R, Schlauch D, Quackenbush J. RNA-Seq analysis in MeV. Bioinformatics 2011; 27:3209-10.

32. Team RC. Place R Foundation for Statistical Computing: R Foundation for Statistical Computing; 2021.

33. Hasegawa K, Sato A, Tanimura K, Uemasu K, Hamakawa Y, Fuseya Y, et al. Fraction of MHCII and EpCAM expression characterizes distal lung epithelial cells for alveolar type 2 cell isolation. Respir Res 2017; 18:150.

34. Rube CE, Uthe D, Schmid KW, Richter KD, Wessel J, Schuck A, et al. Dose-dependent induction of transforming growth factor beta (TGF-beta) in the lung tissue of fibrosis-prone mice after thoracic irradiation. Int J Radiat Oncol Biol Phys 2000; 47:1033-42.

35. Rube CE, Uthe D, Wilfert F, Ludwig D, Yang K, Konig J, et al. The bronchiolar epithelium as a prominent source of pro-inflammatory cytokines after lung irradiation. Int J Radiat Oncol Biol Phys 2005; 61:1482-92.

36. Schaue D, McBride WH. Links between innate immunity and normal tissue radiobiology. Radiat Res 2010; 173:406-17.

37. Shapiro D, Finkelstein J, Penney DP, Siemann D, Rubin P. Sequential Effects of Irriadiation on the Pulmonary System. Int J Radiat Oncol Biol Phys 1982; 8:879-82.

38. He Y, Thummuri D, Zheng G, Okunieff P, Citrin DE, Vujaskovic Z, et al. Cellular senescence and radiation-induced pulmonary fibrosis. Transl Res 2019; 209:14-21.

39. Koukourakis MI, Kyrias G, Kakolyris S, Kouroussis C, Frangiadaki C, Giatromanolaki A, et al. Subcutaneous administration of amifostine during fractionated radiotherapy: a randomized phase II study. J Clin Oncol 2000; 18:2226-33.

40. Komaki R, Lee JS, Milas L, Lee HK, Fossella FV, Herbst RS, et al. Effects of amifostine on acute toxicity from concurrent chemotherapy and radiotherapy for inoperable non-small-cell lung cancer: report of a randomized comparative trial. Int J Radiat Oncol Biol Phys 2004; 58:1369-77.

41. Pan J, Li D, Xu Y, Zhang J, Wang Y, Chen M, et al. Inhibition of Bcl-2/xl With ABT-263 Selectively Kills Senescent Type II Pneumocytes and Reverses Persistent Pulmonary Fibrosis Induced by Ionizing Radiation in Mice. Int J Radiat Oncol Biol Phys 2017; 99:353-61.